Photochemical & Photobiological Sciences

Cite this: *Photochem. Photobiol. Sci.*, 2012, **11**, 803

www.rsc.org/pps

PAPER

Long-distance energy transfer photosensitizers arising in hybrid nanoparticles leading to fluorescence emission and singlet oxygen luminescence quenching

Aymeric Sève,[a] Pierre Couleaud,[a] François Lux,[b] Olivier Tillement,[b] Philippe Arnoux,[a] Jean-Claude André[a] and Céline Frochot[a]

Received 30th September 2011, Accepted 25th January 2012
DOI: 10.1039/c2pp05324a

This paper presents energy transfer occurring in small organically modified core–shell nanoparticles (core lanthanide oxide, shell polysiloxane) (diameter < 10 nm) conjugated with photosensitizers designed for photodynamic therapy applications. These nanoparticles covalently encapsulate a photosensitizing PDT drug in different concentrations. Stable dispersions of the nanoparticles were prepared and the photophysical properties of the photosensitizers were studied and compared to those of the photosensitizers in solution. Increasing the photosensitizer concentration in the nanoparticles was not found to cause any changes in the absorption properties while fluorescence and singlet oxygen quantum yields decreased. As a possible explanation, we have suggested that both long distance energy transfer such as FRET and self-quenching could occur into the nanoparticles. A simple "trend" model of this kind of energy transfer complies with results of experiments on steady state fluorescence and singlet oxygen luminescence.

1. Introduction

Photodynamic therapy (PDT) is one of the non-invasive ways of treating malignant tumors or macular degeneration.[1,2] After light excitation, the photosensitizer (PS) is promoted to the excited singlet state decays to the triplet state and generates highly reactive oxygen species (ROS) such as singlet oxygen through intermolecular triplet–triplet energy transfer to oxygen. The ROS produced are toxic to cells and tissues and destroy cancer cells.[3,4]

As we have previously suggested, non-biodegradable nanoparticles (NPs) seem to be very promising carriers satisfying all the requirements for an ideal targeted PDT.[5,6] It has also been suggested that hybrid gadolinium oxide nanoparticles are useful for magnetic resonance imaging (MRI) and treatment[7–9] because of their small size (less than 50 nm of diameter), their polysiloxane shell, which allows the covalent coupling of a photosensitizer, and the fact that their polyethylene glycol (PEG) grafting allows the covalent coupling of peptide units, thus making them an ideal nanoplatform for both imaging and PDT. We also investigated the influence of the length of different PEG on the biodistribution of hybrid gadolinium oxide NPs.[9] In this targeting strategy using nanomaterials, we conjugated a chlorin, 5-(4-carboxyphenyl)-10,15,20-triphenyl-chlorin (TPC) and the ATWLPPR heptapeptide to a hybrid gadolinium oxide nanoparticle. We studied its functionalization and photophysical properties as well as cytotoxicity and *in vitro* photodynamic efficiency, describing for the first time the molecular affinity of the functionalized NP to NRP-1 molecular target.[10]

Aggregation is important in PDT because it occurs readily between photosensitizer molecules in water-rich media and the photophysical properties of aggregate species are different from those of the monomer. In particular, the aggregate is usually found to have lower singlet oxygen quantum yield and therefore a lower photodynamic efficacy induced by non-fluorescent dimers.[11] By covalently coupling the photosensitizer into a nanoparticle, it is thus possible to avoid aggregation. Nevertheless, if the loading is too high, this may result in interaction between PS units and a self-inhibition.

In this paper, we shall focus on the influence of the concentration of photosensitizer covalently linked into a nanoparticle onto the photophysical properties of the PSs. We showed experimentally and by elaborating a model that by increasing photosensitizer concentration we induced a Förster resonance energy transfer (FRET) associated with partial quenching linked to the formation of dimers or complexes.

2. Materials and methods

2.1. Chemistry

Gadolinium chloride salt (3.346 g, $GdCl_3{\cdot}6H_2O$) and terbium chloride salt (3.360 g, $TbCl_3{\cdot}6H_2O$) (1 : 1) were placed in

[a]*LRGP, Laboratoire Réactions et Génie des Procédés, UPR 3349 CNRS, Nancy, France*
[b]*LPCML, Laboratoire de Physico Chimie des Matériaux Luminescents (LPCML), UMR 5620 CNRS, Lyon, France. E-mail: celine.frochot@ensic.inpl-nancy.fr; Fax: + 33 3 83 37 81 20; Tel: + 33 3 83 17 15 15*

120 mL of diethylene glycol (DEG) at room temperature with vigorous stirring. The suspension was heated at 180 °C until the total dissolution of lanthanide salts (about 1 h). When the solution was clear, sodium hydroxide solution (4 mL, 4.06 M) was added drop-by-drop with vigorous stirring again. Afterwards, the solution was heated and stirred at 180 °C for 3 hours. A transparent colloid of lanthanide oxide nanoparticles was obtained and stored at room temperature for weeks without alteration.

A solution containing TPC–NHS (40 mg) and 24.6 µL of aminopropyltriethoxysilane (APTES) dissolved in 8.4 mL of anhydrous dimethyl sulfoxide (DMSO) was stirred during 2 hours to prepare the TPC–APTES precursor. The silane precursors (APTES (3.0 mL) and tetraethoxysilane (TEOS) (2.0 mL)) and hydrolysis solution (aqueous Et_3N in DEG (3.12×10^{-6} M of TEA, 0.15 M of water)) were sequentially and alternatively added to 120 mL DEG solution containing Gd_2O_3–Tb_2O_3 (50/50) nanoparticles ([Ln] = 45 mM) under stirring at 40 °C. Addition of silane precursors and hydrolysis solution was performed in 6 steps. Each step consisted of the addition to the colloid of a portion of the silane precursor mixture followed by the addition of hydrolysis solution mixture. The solution containing the TPC coupled to the APTES (TPC–APTES) was added in the first step in addition to the other silane precursors (respectively 5, 10, 20 and 50 eq. TPC–APTES/Gd_2O_3–Tb_2O_3 core to synthesize nano5, nano10, nano20 and nano50). There was a one hour delay between the two additions. After the last addition, the final mixture was stirred for 48 h at 40 °C.

Direct measurements of the size distribution of the nanoparticles were performed using photon correlation spectroscopy with Zetasizer NanoZS90 (He–Ne red laser 633 nm, 50 mW) (Malvern Instrument). Size measurements were carried out in deionized water with the colloids after purification by dialysis.

2.2. Photophysical properties

Absorption spectra were recorded on a Perkin-Elmer (Lambda 2, Courtaboeuf, France) UV-visible spectrophotometer. Fluorescence spectra were recorded on a SPEX Fluorolog-3 spectrofluorimeter (Jobin & Yvon, Longjumeau, France) equipped with a thermo stated cell compartment (25 °C), using a 450 W xenon lamp. Fluorescence quantum yields (Φ_f) were determined using a tetraphenyl porphyrin solution as a fluorescence standard (Φ_f = 0.11, in toluene, taking into account solvent refractive index and absorption efficiencies).[12] For the direct determination of $^1O_2$ quantum yield (Φ_Δ) excitation occurred with a Xe-arc, the light was separated in a SPEX 1680, 0.22 µm double monochromator. The detection at 1270 nm was carried out through a PTI S/N 1565 monochromator, and the emission was monitored by a liquid nitrogen-cooled Ge-detector model (EO-817L, North Coast Scientific Co.). Rose Bengal was chosen as a reference solution thanks to its high $^1O_2$ quantum yield in EtOH (Φ_Δ = 0.68[13]). The absorbance value at the excitation wavelength (414 nm) of both the reference (Rose Bengal) and the nanoparticles solutions were set to around 0.2 by dilution.

3. Results and discussion

3.1. Experimental results

We synthesized silica nanoparticles with different amounts of covalently bound photosensitizers. We added a carboxylic tetraphenyl chlorin that had previously been activated with a NHS group to aminopropyltriethoxysilane (APTES) to prepare the TPC–APTES precursor. The precursor was added in the first step in addition to the other silane precursors to the Gd_2O_3–Tb_2O_3 (50 : 50) NPs. By modulating the quantity of TPC–APTES, we synthesized nanoparticles with theoretically 5, 10, 20 or 50 equivalents of TPC by NP (called respectively nano5, nano10, nano20, nano50). Because the coupling was not total, the number of PS units coupled to the nanoparticles was estimated by comparing the absorption at 420 nm of the TPC coupled to the NP to an absorption calibration curve of the TPC in solution. For each NP (nano5, nano10, nano20, nano50), the coupling of the PS was around 30%. The hydrodynamic radius was estimated by PCS on the nanoparticles with no PS because of the interaction between the PS (absorption at 633 nm) and the laser used to determine the size of the particles. The same manipulations on nanoparticles performed with a fluorescein fluorophore (with no absorption at 633 nm) were found to lead to only negligible diameter variations. A diagram summing up the reaction is given in Fig. 1.

We compared the photophysical properties of the TPC coupled to nano5, nano10, nano20 and nano50 for the same concentration of nanoparticles in a solution. The absorption spectra of TPC in the NPs are presented in Fig. 2.

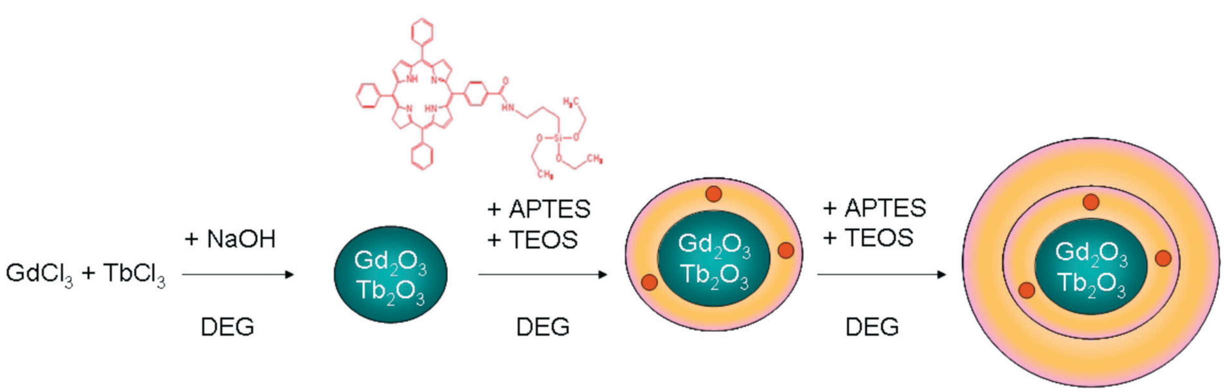

Fig. 1 Diagram of the reaction.

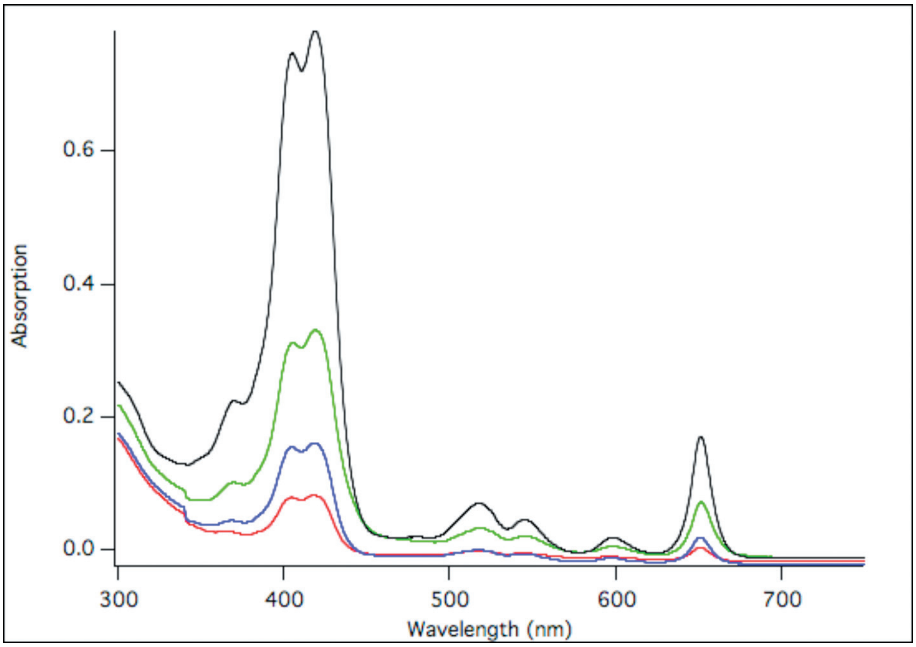

Fig. 2 Absorption spectra of TPC covalently coupled to a same concentration of nanoparticles in ethanol (red: nano5, blue: nano10, green: nano20, black: nano50).

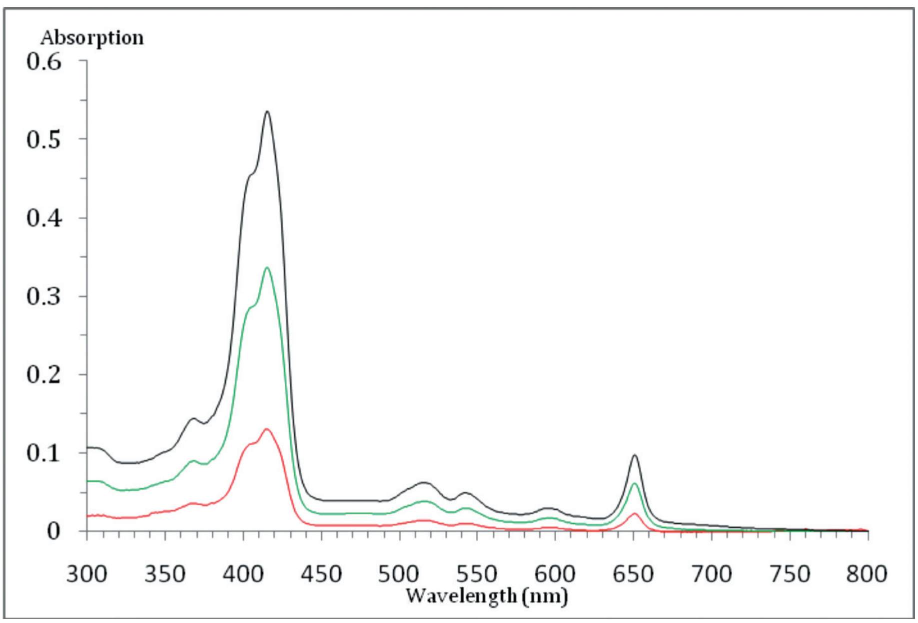

Fig. 3 Absorption spectra of TPC in ethanol (red: 7.7×10^{-7} mol L^{-1}, green: 2×10^{-6} mol L^{-1}, black: 3.2×10^{-6} mol L^{-1}).

They consist of one strong absorption peak caused by $S_0 \rightarrow S_{n>2}$ (B or Soret band) transitions closed to 420 nm. Besides Soret band, four weak Q bands caused by two $S_0 \rightarrow S_1$ (Q_x bands) and two $S_0 \rightarrow S_2$ (Q_y bands) transitions are observed between 500 and 650 nm. The intensity ratio of these four Q-bands shows an ethio type spectrum. The absorption spectrum exhibits a minimal light scattering contribution, thanks to the small size of the nano-objects (Rayleigh and/or Mie scattering). The UV-visible spectra are composed of light absorption due to the chlorin chromophore as well as an absorption associated with the GdTb core of the nanoparticle, around 300 nm. Increasing the concentration of TPC into the nanoparticles was not found to induce any apparent change in the shape and any shift of the UV-visible spectra. The same phenomenon is observed for free TPC in solution – the increase of the concentration has no effect on the shape of UV-visible spectrum in this concentration range (Fig. 3).

As expected, Fig. 4 shows that the absorption at 420 nm of TPC in nano5, nano10, nano20 or nano50 is proportional to the concentration of TPC into the nanoparticles.

The shapes of the fluorescence spectra of free TPC and TPC coupled to the nanoparticles are similar and the maximum $S_{1,0} \rightarrow S_{0,0}$ is detected at 650 nm (Fig. 5). Another small band can be observed at 720 nm as already shown previously.[14]

Fig. 6 shows the fluorescence intensity according to the TPC concentration for TPC in solution or coupled to the nanoparticles. The fluorescence emission of TPC in solution was proportional to the absorbance at low concentration (no skin effect) but the fluorescence intensity of the TPC coupled to the NP was found to decrease when the concentration of TPC increased.

We measured the formation of singlet oxygen by recording direct luminescence of $^1O_2$ after excitation of the TPC at 414 nm (Fig. 7).

While the $^1O_2$ formation of TPC in solution was proportional to the absorption at low concentration (no skin effect), the $^1O_2$ formation of the TPC coupled to the nanoparticles decreased when the concentration of TPC increased (Fig. 8).

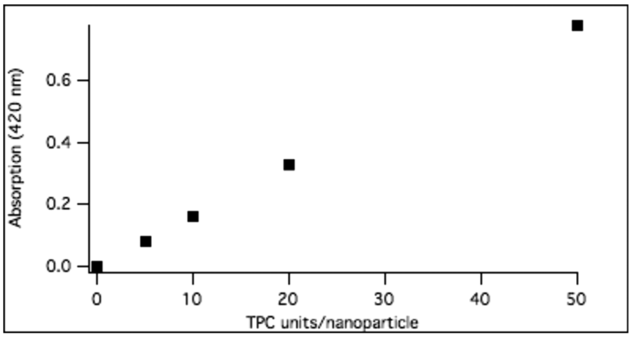

Fig. 4 TPC absorption at 420 nm in ethanol of nano5, nano10, nano20, nano50 (number of units per nanoparticle based on the synthesis, same concentration).

These results suggest there was a quenching due to the increasing concentration of TPC units into the nanoparticles. In order to explain the results, different phenomenon could be taken into account:

• The formation of a complex in the ground state. Since the UV spectra apparently do not change, this hypothesis should be not retained.

• A quenching by an inhibitor present in the bulk. The effect has to be independent from the number (n) of the photosensitizers units coupled to the nanoparticle.

• Long-distance energy transfer such as FRET: if this mechanism were to occur alone, there would be only a delocalization of electronic energy onto the photosensitizers without in principle, a loss of energy. At the same time, the yield of $^1O_2$ production will probably be improved if a non-stationary diffusion controlled reaction between the TPC singlet state and oxygen occurs.[15] This was not observed experimentally.

• Both long-distance energy transfer such as FRET and a quenching process. If we suppose that the photosensitizer is localized in close proximity to a quencher Q, the diffusion at molecular scale of the electronic energy to the quenching site could result in a decrease of fluorescence.

3.2. Simplified model

To validate the kinetics results, we developed a simplified model based on the following assumptions:

• All the nanoparticles are mono disperse (no light dispersion).

• For a given concentration of PS, the number of PS is identical in each monodisperse nanoparticle.

• The distribution of the photosensitizer is assumed to be homogenous into each NP.

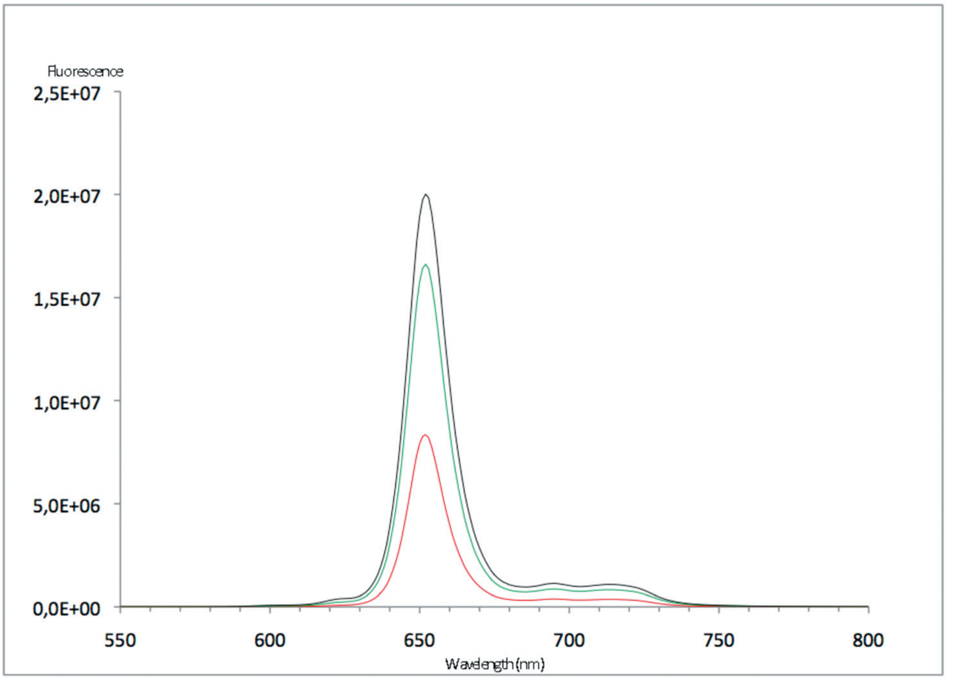

Fig. 5 Fluorescence spectra of TPC in ethanol (red: 7.7×10^{-7} mol L^{-1}, green: 2×10^{-6} mol L^{-1}, black: 3.2×10^{-6} mol L^{-1}).

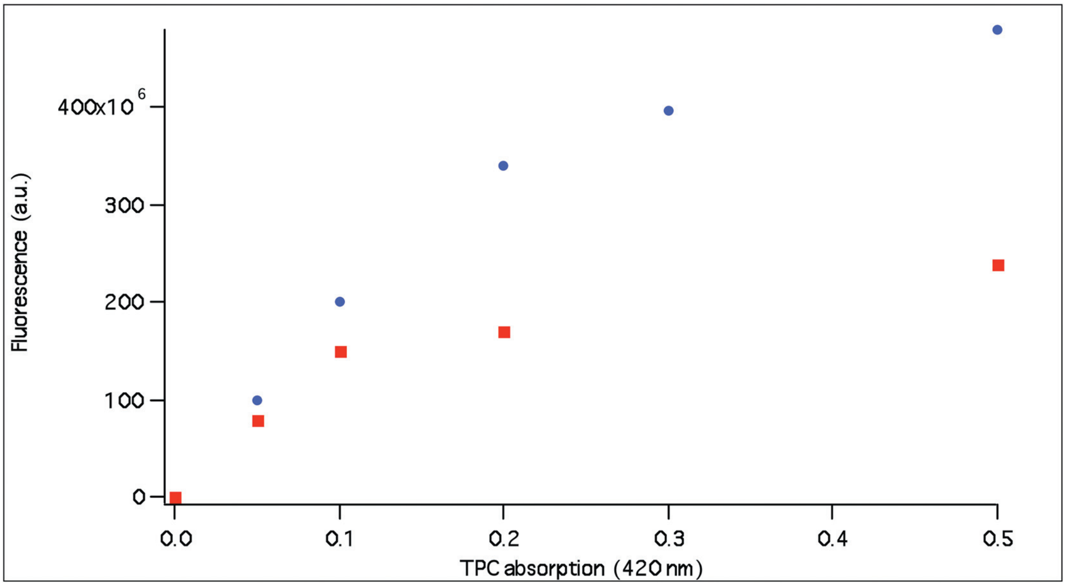

Fig. 6 Fluorescence intensity in function of the TPC concentration of free TPC (blue) and of TPC covalently coupled to the nanoparticles (red).

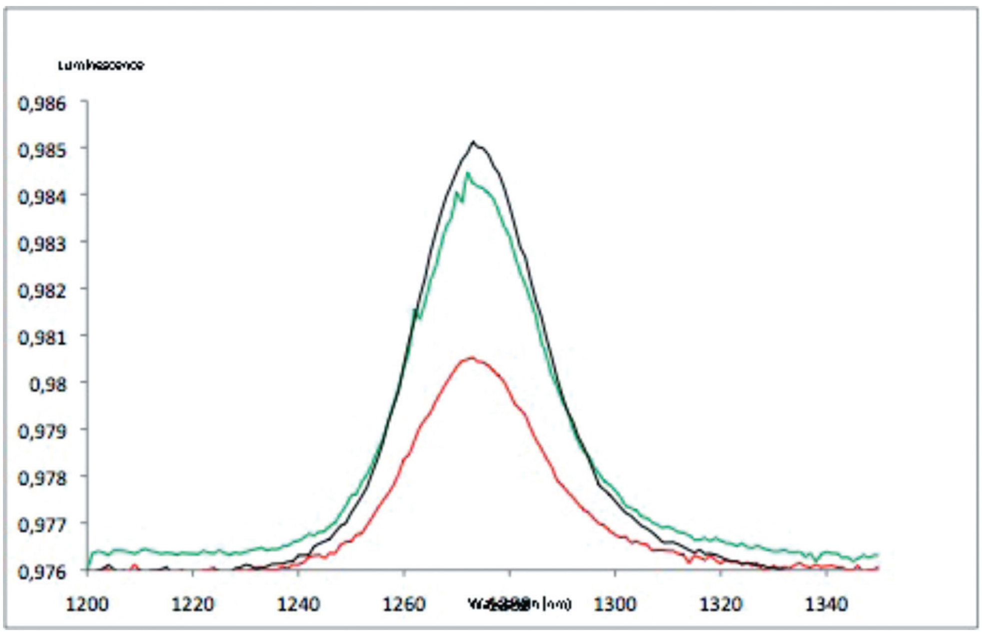

Fig. 7 Singlet oxygen formation of TPC in ethanol (red: 7.7×10^{-7} mol L^{-1}, green: 2×10^{-6} mol L^{-1}, black: 3.2×10^{-6} mol L^{-1}, $\lambda_{exc} = 414$ nm).

It is then possible to write:

$$PS \rightarrow PS*$$

$$PS * + PS \rightarrow PS + PS * \quad \text{(spatial delocalization of the electronic state onto the nanoparticles)}$$

$$PS * + Q \rightarrow \text{inhibition/quenching}$$

Taking into account the possible long-distance energy transfer (Förster mechanism), when the number of covalently grafted PS increases in the nanoparticles the average distance between two PS decreases. It might be possible that for distances closer to the Förster distance R_0 electronic energy transfer could move the energy around the particles (Fig. 9). The photosensitizer's S_1 electronic state created at time $t = 0$ can migrate from one position to another PS_1*, PS_2*, PS_3*, *etc.*

If no other quenching occurs, the lifetime of the PS must be constant and independent of the number of PS per nanoparticle. This theoretical hypothesis has not been tested by experiments. Nevertheless, the value R_0 has been determined by absorption and emission spectroscopies and is of the order of magnitude of 50 Å, which is larger than the diameter of the nanoparticle. In this respect, Förster energy transfer seems to be a possible mechanism for energy delocalization onto the nanoparticle.

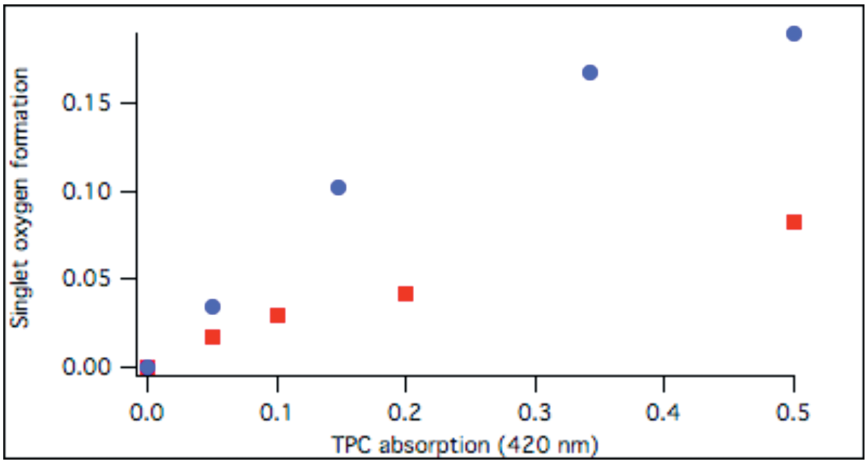

Fig. 8 Singlet oxygen luminescence intensity in function of the TPC concentration of free TPC (blue) and of TPC covalently coupled to the nanoparticles (red).

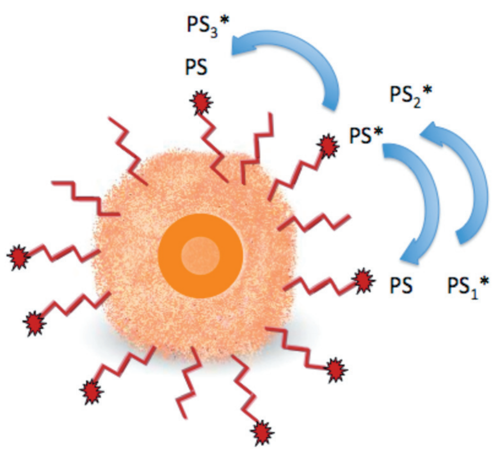

Fig. 9 Schematic of structure and mechanism of action of quenching in the nanoparticles.

Following on from the above comment, if a quencher Q is present on the surface of the particle (Fig. 9) the migration of the electronic energy may induce the formation of an excited PS* close to a quencher, leading to the observed quenching. The simple modeling presented here is defined by assuming the following statements:

• The energy transfer between PS* and PS in the ground state with a rate defined by Förster mechanism.

• Static quenching when a PS* is located to a quencher Q.

• Regarding the transport process of the electronic energy ($PS^*_i \rightarrow PS^*_{i+1}$) as close to the conceptual vision of a diffusion-controlled process (random displacements of the electronic energy) leading to a classical rate constant of reactions defined by:[16]

$$k_Q = \alpha \pi N \sigma D \tag{1}$$

where σ is the collision distance between the donor and the acceptor, α is a coefficient relative to the space for the reaction (4 for a spherical symmetry, 2 for a spherical surface, *etc.*).

It is possible to define the apparent inhibition quenching rate constant with such a diffusion process of electronic energy transfer (effective in absence of molecular transfer) using the following data:

• Surface of the nanoparticle: $4\pi r^2$.

• The average surface occupied by a single photosensitizer: $4\pi r^2/n$ with n being the number of PS per nanoparticle.

• The average distance between 2 photosensitizers:

$$R = 2\sqrt{(4\pi r^2/n)} = 4r\sqrt{(\pi/n)} \tag{2}$$

• The rate constant k of a Förster type energy transfer process is

$$k = k_0 (R_0/R)^6 \tag{3}$$

where R_0 is the classical Förster distance.

By analogy, the apparent D electronic energy "diffusion" coefficient is:

$$D = R^2 k \tag{4}$$

From (1) and (4),

$$k_Q = \alpha \pi N \sigma R^2 k \tag{5}$$

From (3) and (5), σ = R:

$$k_Q = \alpha \pi N \times R \times R^2 \times k_0 (R_0/R)^6 = \alpha \pi N k_0 {R_0}^6 R^{-3}$$

$$k_Q = K R^{-3} \tag{6}$$

with $K = \alpha \pi N k_0 {R_0}^6$.

And finally from (6) and (2),

$$k_Q = K(4r\sqrt{(\pi/n)})^{-3} = K' n^{-3/2} \tag{7}$$

with $K' = K^*(4r^*\sqrt{(\pi)})^{-3}$.

The fluorescence quantum yield (Φ_f) can be written as (Stern–Volmer plots):

$$\Phi_{f0}/\Phi_f = 1 + k_Q \tau_N [Q] \tag{8}$$

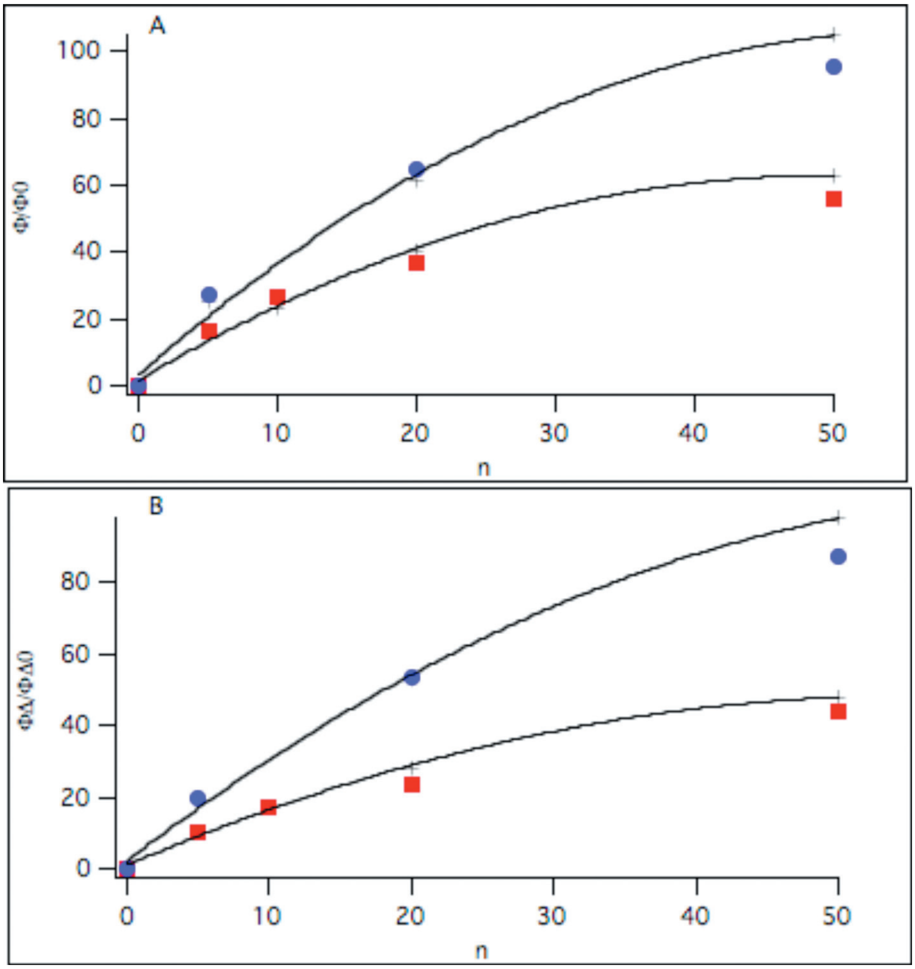

Fig. 10 (A) Φ_{f0}/Φ_f in function of n. (B) $\Phi_{\Delta 0}/\Phi_\Delta$ in function of n. Experimental data in red: TPC coupled to the nanoparticles, blue: TPC in solution. Black: fitting using a least square simplified techniques.

where Φ_{f0} is the fluorescence quantum yield without any quencher, τ_N is the natural fluorescence lifetime of the photosensitizer. From a hypothetical standpoint, if the light absorbed by a photosensitizer is independent of the distance to the quencher Q, at $t = 0$, the light is uniformly distributed around the quencher Q.

From (7) and (8),

$$\Phi_{f0}/\Phi_f = 1 + K'\tau_N n^{3/2}[Q]$$

with $K' = K(4r\sqrt{(\pi)})^{-3}$.

In Fig. 10, after a classical fitting using a simplified least-square technique we reported Φ_{f0}/Φ_f and $\Phi_{\Delta 0}/\Phi_\Delta$ in function of n.

This experimental data complies with our proposed model. At the same time, we showed that $^1O_2$ production evolved in the same manner. Fluorescence emission and $^1O_2$ production have in this respect the same origin.

Both our fluorescence experiments and formation using a classical model for the definition of the skin effect on the analyzed signal showed that, for the highest concentrations of PS, the calculated curve is always located at lower values than the experimental ones. Independently of the quality of the measurements, this result is possibly explained by an effect of some self-quenching induced by the formation of dimers in the ground state.

3.3. Discussion

Most conventional photosensitizers form aggregates due to their π–π interactions and hydrophobic characteristics resulting in significant reduction of singlet oxygen by self-quenching. Indeed, aggregation shortens the triplet-state lifetime and decreases the singlet oxygen quantum yield by dissipating energy through internal conversion.[17–19] However, this property has been used by different research teams to target singlet oxygen formation given that aggregated PSs are non-toxic and become phototoxic when released in their monomeric form. These carrier systems have a switching phototoxicity. For example, McCarthy *et al.*[20] showed that some aggregated PSs loaded in biodegradable nanoparticles are stable and non-phototoxic upon systemic administration. Upon cellular internalization, the PS is released from the nanoparticle and becomes highly phototoxic. Other teams have developed smart and complex molecules that can be activated in the presence of enzymes that are specific to cancer cells, tumour medium or metastatic activity.[21–24]

As we previously described, non-biodegradable nanoparticles also seem to be a very promising option satisfying all the requirements for an ideal targeted PDT and can be used to improve the targeting of the photosensitizer.[5,6] It has been suggested that hybrid gadolinium oxide nanoparticles could be useful for magnetic resonance imaging (MRI) and treatment.[7–9] Their small size (less than 50 nm of diameter), their silica shell that allows the covalent coupling of a photosensitizer, and their polyethylene glycol (PEG) grafting that allows the covalent coupling of peptide units all make them an ideal nanoplatform for both imaging and PDT.

In these nanoparticles, the PS is covalently coupled to the NP. To be efficient, it is essential that photosensitizers keep their photophysical properties after their covalent coupling to the NP. In a first study[10] we proved that it was possible to elaborate multifunctional nanoparticles that present photodynamic activity. Using the fluorescence of the photosensitizer, we could estimate that each nanoparticle contains around 6 chlorin molecules. The signature phosphorescence emission of $^1O_2$ at 1270 nm was clearly observed. We could also observe a very low decrease in the NP fluorescence emission and singlet oxygen emission indicated that the photosensitizer molecules linked into the silica matrix were slightly affected by the microenvironment.

To develop the most appropriate nanoparticles for effective PDT applications, in this study we looked at the influence of the number of PS grafted onto the nanoparticles on the photophysical properties. Indeed, the multigrafting of PS onto a nanoparticle can create a ground state complex such as dimers. In this respect, according to previous works in this field, when an excited PS transfer its electronic energy into such a weak complex a non-reversible energy transfer will occur leading to lose a part of the electronic energy and $^1O_2$ production. Basic understanding of dye aggregation on a nanoparticle surface as well as the excited state interaction with a semiconductor support was studied by Barazzouk *et al.*[25] They investigated the photoelectrochemical properties of carbocyanine dyes adsorbed on SnO_2 and SiO_2 surfaces. The authors observed a blue shift in the absorption maximum upon adsorption of the dye molecules on SnO_2 and SiO_2 colloids surfaces, supporting the argument that monomer and aggregates forms of dye were in equilibrium. They proved that the binding of cyanine dye molecules to SnO_2 and SiO_2 colloid surfaces induced intermolecular interactions leading to an aggregation effect, and the blue shift in absorption bands confirmed the dye aggregation to be of H-type.

More recently, Rossi's team developed protoporphyrin IX nanoparticle carriers, and studied the photophysical properties of this well-known photosensitizer.[26] They synthesized an organosilane protoporphyrin IX and coupled it to a nanoparticle-based system. Firstly, a red shift of the Soret band of silyl-functionalized PpIX compared to PpIX was observed and the authors suggested this was due to a decrease in aggregation. The absorption spectra corresponding to the Soret and the Q bands in the porphyrin absorption spectrum were also observed in a suspension of PpIX-loaded silica spheres, although the bands were overlapped by the light scattering of solid particles (mean particle diameter 77 ± 12 nm). Emission bands of the PpIX-loaded silica particles in aqueous solution were slightly shifted to the blue region as compared to the emission spectrum of silyl-PpIX free in aqueous solution. Generation of $^1O_2$ was more efficient for the PpIX encapsulated than for the free PpIX. This was attributed to a decrease in the monomer–dimer equilibrium because the porphyrin is covalently attached to the silica matrix, while in solution this kind of equilibrium is possible leading to a decrease of $^1O_2$ quantum yield. Based on these promising results, the same team recently published a paper about silica gel nanoparticles containing phenothiazine photosensitizer with specific ratios of dimer to monomer species (methylene blue and thionin).[27] By recording the absorption spectra, the authors could estimate the ratio dimer–monomer. As expected, they observed a decreasing amount of $^1O_2$ generation with a decrease of the dimer–monomer ratios.

In our study, we synthesized nanoparticles coupled with different amount of PSs with an estimated coupling yield of 30%. For obvious topological reasons, it seems difficult to increase the number of PS units on each nanoparticle after a certain limit. Whereas the absorption spectra of the photosensitizer were not affected by an increase of the chlorin concentration, both fluorescence emission and singlet oxygen emission were found to decrease when the concentration of covalently linked PSs increased. The decrease of $^1O_2$ quantum yield has been observed by other authors,[28,29] suggesting that this may be due to indirect effects such as the scattering of the nanoparticles, the local sequestration of generated $^1O_2$ by the NP matrix or by intrinsic lower encapsulated photosensitizer $^1O_2$ quantum yield. Since the nanoparticles are the same size, and the polysiloxane is the same matrix, these hypotheses do not appear to be true according to our system. By elaborating a model to interpret this phenomenon, we would rather suggest the influence of both long distance energy transfer such as FRET and inhibition by PS ground state dimer. From an application standpoint, increasing the concentration of grafted TPC into the nanoparticles leads to a quenching effect of fluorescence and $^1O_2$ luminescence.

4. Conclusion

Covalent coupling of photosensitizers into nanoparticles offer a real advantage for PDT applications given that the photosensitizers cannot, in practise, be released from the nanoparticles and are protected from their environment. The grafting of a large number of PS onto a nanoparticle may still therefore be considered a highly interesting option for cancer treatment through PDT. Nevertheless, our work proved that the amount of covalently grafted PS has a slightly negative influence on the fluorescence and singlet oxygen quantum yields. If the payload is too high, this may result in a decrease of singlet oxygen quantum yield due to FRET associated with partial quenching linked to the formation of dimers.

Abbreviations

APTES	Aminopropyltriethoxysilane
Ce6	Chlorin e6
DEG	Diethyleneglycol
DMSO	Dimethylsulfoxide
FRET	Förster resonance energy transfer
Φ_F	Fluorescence quantum yield
Φ_Δ	Singlet oxygen quantum yield
MRI	Magnetic resonance imaging

NHS	*N*-Hydroxy succinimic ester
PDT	Photodynamic therapy
PEG	Polyethylene glycol
PS	Photosensitizer
Q	Quencher
ROS	Reactive oxygen species
TEA	Triethylamine
TEOS	Tetraethoxysilane
TPC	5-(4-Carboxyphenyl)-10,15,20-triphenylchlorin

References

1 R. K. Pandey and G. Zhang, *Porphyrin Handbook*, ed. K. M. Kadish, K. M. Smith, R. Guilard, Academic Press, San Diego, CA, 2000.

2 I. J. MacDonald and T. J. Dougherty, Basic principles of photodynamic therapy, *J. Porphyrins Phthalocyanines*, 2001, **5**, 105–129.

3 K. R. Weishaupt, C. J. Gomer and T. J. Dougherty, Identification of singlet oxygen as the cytotoxic agent in photo inactivation of a murine tumor, *Cancer Res.*, 1976, **36**, 2326–2329.

4 J. B. Mitchell, S. McPherson and W. DeGraff, Oxygen dependence of hematoporphyrin derivative-induced photoinactivation of Chinese hamster cells, *Cancer Res.*, 1985, **45**, 2008–2011.

5 D. Bechet, P. Couleaud, C. Frochot, M. L. Viriot, F. Guillemin and M. Barberi-Heyob, Nanoparticles as vehicles for delivery of photodynamic therapy agents, *Trends Biotechnol.*, 2008, **26**, 612–621.

6 D. Brevet, M. Gary-Bobo, L. Raehm, S. Richeter, O. Hocine, K. Amro, B. Loock, P. Couleaud, C. Frochot, A. Morère, P. Maillard, M. Garcia and J. O. Durand, Mannose-targeted mesoporous silica nanoparticles for photodynamic therapy, *Chem. Commun.*, 2009, 1475–1477.

7 J. L. Bridot, A. C. Faure, S. Laurent, C. Rivière, C. Billotey, B. Hiba, M. Janier, V. Josserand, J. L. Coll, L. Vander Elst, R. Muller, S. Roux, P. Perriat and O. Tillement, Hybrid gadolinium oxide nanoparticles Multimodal contrast agents for in vivo imaging, *J. Am. Chem. Soc.*, 2007, **129**, 5076–5084.

8 A. C. Faure, S. Dufort, V. Josserand, P. Perriat, J. L. Coll, S. Roux and O. Tillement, Control of the in vivo biodistribution of hybrid nanoparticles with different poly(ethylene glycol) coating, *Small*, 2009, **5**, 2565–2575.

9 A. C. Faure, C. Hoffmann, R. Bazzi, F. Goubard, E. Pauthe, C. A. Marquette, L. J. Blum, S. Roux and O. Tillement, Functionalization of luminescent aminated particles for facile bioconjugation, *ACS Nano*, 2008, **2**, 2273–2282.

10 P. Couleaud, D. Bechet, R. Vanderesse, M. Barberi-Heyob, A. C. Faure, S. Roux, O. Tillement, S. Porhel, F. Guillemin and C. Frochot, Functionalized silica-based nanoparticles for photodynamic therapy, *Nanomedicine*, 2011, **6**, 995–1009.

11 R. Bonnett, *Chemical Aspect of Photodynamic Therapy*, Gordon and Breach Science Publisher, 2000.

12 T. L. C. Figueiredo, R. A. W. Johnstone, A. M. P. SantAna Sørensen, D. Burget and P. Jacques, Determination of fluorescence yields, singlet lifetimes and singlet oxygen yields of water-insoluble porphyrins and metalloporphyrins in organic solvents and in aqueous media, *Photochem. Photobiol.*, 1999, **69**, 517–528.

13 M. C. Derosa and R. J. Crutchley, Photosensitized singlet oxygen and its applications, *Coord. Chem. Rev.*, 2002, **233–234**, 351–371.

14 L. Tirand, C. Frochot, R. Vanderesse, N. Thomas, E. Trinquet, S. Pinel, M. L. Viriot, F. Guillemin and M. Barberi-Heyob, A peptide competing with VEGF165 binding on neuropilin-1 mediates targeting of a chlorin-type photosensitizer and potentiates its photodynamic activity in human endothelial cells, *J. Controlled Release*, 2006, **111**, 153–164.

15 W. Dong and J. C. André, Diffusion-controlled reactions. II. An approach based on generalized diffusion equation, *J. Chem. Phys.*, 1994, **101**, 299–306.

16 J. Perrin, Mouvement brownien et réalité moléculaire, *Ann. Chim. Phys.*, 1909, **19**, 5–104.

17 L. E. Bennett, K. P. Ghiggino and R. W. Henderson, Singlet oxygen formation in monomeric and aggregated porphyrin c, *J. Photochem. Photobiol., B*, 1989, **3**, 81–89.

18 X. Damoiseau, H. J. Schuitmaker, J. W. M. Lagerberg and M. Hoebeke, Increase of the photosensitizing efficiency of the Bacteriochlorin a by liposome-incorporation, *J. Photochem. Photobiol., B*, 2001, **60**, 50–60.

19 M. R. Hamblin, J. L. Miller, I. Rizvi and B. Ortel, Degree of substitution of chlorin(e6) conjugated to charged poly-L-lysine chains affects their cellular uptake, localization and phototoxicity towards macrophages and cancer cells, *J. XRay Sci. Tech.*, 2002, **10**, 139–152.

20 J. R. McCarthy, J. M. Perez, C. Brückner and R. Weissleder, Polymeric nanoparticle preparation that erradicate tumors, *Nano Lett.*, 2005, **5**, 2552–2556.

21 M. Verhille, P. Couleaud, R. Vanderesse, M. Barberi-Heyob and C. Frochot, Modulation of photosensitization processes for an improved targeted photodynamic therapy, *Curr. Med. Chem.*, 2010, **17**, 3925–43.

22 Y. Choi, R. Weissleder and C. H. Tung, Selective antitumor effect of novel protease-mediated photodynamic agent, *Cancer Res.*, 2006, **66**, 7225–7229.

23 M. A. Campo, D. Gabriel, P. Kucera, R. Gurny and N. Lange, Polymeric photosensitizer prodrugs for photodynamic therapy, *Photochem. Photobiol.*, 2007, **83**, 958–965.

24 D. Gabriel, M. F. Zuluaga, M. N. Martinez, M. A. Campo and N. Lange, Urokinaseplasminogen sensitive polymeric photosensitizer prodrugs: Design, synthesis and in vitro evaluation, *J. Drug Deliv. Sci. Tech.*, 2009, **19**, 15–24.

25 S. Barazzouk, H. Lee, S. Hotchandani and P. V. Kamat, Photosensitization aspects of Pinacyanol H-aggregates. Charge injection from singlet and Triplet states into SnO_2 Nanocrystallites, *J. Phys. Chem. B*, 2000, **104**, 3616–3623.

26 L. M. Rossi, P. R. Silva, L. L. R. Vono, A. U. Fernandes, D. B. Tada and M. S. Baptista, Protoporphyrin IX nanoparticle carrier: preparation, optical properties and singlet oxygen generation, *Langmuir*, 2008, **24**, 12534–12538.

27 D. B. Tada, L. M. Rossi, C. A. P. Leite, R. Itri and M. S. Baptista, Nanoparticle Platform to modulate reaction mechanism of phenothiazine photosensitizers, *J. Nanosci. Nanotechnol.*, 2010, **10**, 1–9.

28 F. Liu, X. Zhou, Z. Chen, P. Huang, X. Wang and Y. Zhou, Preparation of purpurin-18 loaded magnetic nanocarriers in cottonseed oil for photodynamic therapy, *Mater. Lett.*, 2008, **62**, 2844–2847.

29 D. B. Tada, L. L. R. Vono, E. L. Duarte, R. Itri, P. K. Kiyohara, M. S. Baptista and L. M. Rossi, Methylene blue-containing silica-coated magnetic particles: A potential magnetic carrier for photodynamic therapy, *Langmuir*, 2007, **23**, 8194–8199.